Munawwar Mohabuth, Andrei Kotousov, Ching-Tai Ng and LR Francis Rose

Implication of changing loading conditions on structural health monitoring utilising guided waves

Smart Materials and Structures, 2018; 27(2):025003-1-025003-12

Implication of changing loading conditions on structural health monitoring utilising guided waves

Munawwar Mohabuth[1], Andrei Kotousov[1*], Ching-Tai Ng[2] and L. R. Francis Rose[3]

[1]School of Mechanical Engineering, The University of Adelaide, Adelaide, SA 5005, Australia.

[2]School of Civil, Environmental and Mining Engineering, The University of Adelaide, Adelaide, SA 5005, Australia.

[3]Aerospace Division, Defence Science and Technology Group, Fishermen's Bend, VIC 3207, Australia.

*Corresponding author. Tel.: +61 8 8313 6385.

E-mail addresses: munawwar.mohabuth@adelaide.edu.au (M. Mohabuth),

andrei.kotousov@adelaide.edu.au (A. Kotousov),

alex.ng@adelaide.edu.au (C-T. Ng)

francis.rose@dst.defence.gov.au (L.R.F. Rose)

Abstract:

Structural health monitoring systems based on guided waves typically utilise a network of embedded or permanently attached sensors, allowing for the continuous detection of damage remote from a sensor location. The presence of damage is often diagnosed by analysing the residual signals from the structure after subtracting damage-free reference data. However, variations in environmental and operational conditions such as temperature, humidity, applied or thermally-induced stresses affect the measured residuals. A previously developed acoustoelastic formulation is extended and employed as the basis for a simplified analytical model to estimate the effect of applied or thermally-induced stresses on the propagation characteristics of the fundamental Lamb wave modes. It is noted that there are special combinations of frequency, biaxial stress ratio and direction of wave propagation for which there is no change in the phase velocity of the fundamental antisymmetric mode. The implication of these results in devising effective strategies to mitigate the effect of stress induced variations in guided-wave damage diagnostics is briefly discussed.

Keywords: Structural Health Monitoring, Damage detection, Acoustoelasticity, Stress mitigation, Lamb waves, Environment and operational conditions.

1. Introduction

Damage diagnostics is often necessary for the safe and efficient operation of civil and mechanical engineering infrastructure. Structural health monitoring (SHM) normally refers to a process for the in-situ monitoring of the integrity of structures using real-time data obtained from a permanently attached or embedded sensor network. Therefore, there is no need for disassembly of the components to be inspected as the sensors are an inherent part of these structures. This approach represents an alternative to traditional time consuming and labour intensive non-destructing evaluation procedures [1-3].

In recent years, significant progress was achieved in the development of SHM techniques utilising guided waves [4-13]. In particular, it was found that Lamb waves, which are guided waves in traction-free plates, can propagate over several metres without significant decay, thereby offering the possibility of interrogating large areas of plate-like structures with a small number of sensors [14-16]. A typical guided wave (GW) based SHM system incorporates a grid of permanently bonded or embedded transducers. One of the transducers (or transmitters) is excited with a tone burst of a few cycles, generating a stress wave that propagates along the structure. The time-domain responses from the transmitter and the receiving transducers are then recorded. This process is then repeated using different transducers as transmitters. The signal remaining after subtraction from damage-free reference data which exceeds the background noise is assumed to be linked to a defect or mechanical damage. However, one of the main contributions to the background noise in real-world situations arises from variations in environmental and operational conditions (EOC) such as temperature [17-21] and loading [22-27]. These contributions will be referred to as noise in the sense that they represent unwanted contributions. They are, however, deterministic contributions that can be predicted and compensated for.

Changing EOC is arguably the main reason why SHM systems, which have been developed and successfully demonstrated in the last two decades in laboratory conditions, often fail to prove their efficiency in the real-world environment. The background noise due to changing EOC can interfere with the operation of SHM systems leading to false alarms or to the prevention of the critical damage from being detected in service. One way to address this problem is to increase the number of sensors, which however can adversely affect the cost, weight and power efficiency of the SHM system. For example, Croxford et al. [28] demonstrated that in the presence of even modest temperature fluctuations, the number of sensors required for damage detection can be prohibitively

high. Therefore, some form of compensation for changing EOC is often essential for guided wave based SHM systems to be viable [29,30].

The effect of temperature variations on damage detection has been extensively documented in literature over the past two decades. Subsequently, a large effort has been recently directed to the development of various temperature compensation techniques [31-38]. The current paper is focused on the noise generation due to variations in applied or thermally induced stresses. It is shown that the effect of these variations on the noise generation can be comparable with that of moderate temperature fluctuations. Therefore, both effects need to be considered when developing SHM systems for real-world applications. Another interesting outcome of this work is the identification of certain combinations of frequency, biaxial stress ratio and wave propagation direction, for which the applied stress has a minor effect on the phase velocity of the fundamental antisymmetric mode (A0). Favourable operating points for the fundamental symmetric mode (S0) are also discussed. These combinations can provide a basis for developing stress mitigation techniques, which might be necessary to comply with cost, energy or weight constraints for the SHM system.

The current paper is structured as follows. In Section 2, we review the fundamentals of the theory of acoustoelasticity following the work of Ogden [39]. This formulation is then used to derive dispersion equations for Lamb waves propagating along a non-principal direction in a plate subjected to biaxial stresses. In Section 3, we provide numerical results to demonstrate the effect of the applied stress, the propagation direction and the frequency on the propagation of the fundamental Lamb wave modes. Then, in Section 4, we present an analytical model to quantify the noise due to the applied stress and compare the noise levels due to temperature variations and thermally-induced stresses. Finally, in Section 5, we propose different strategies to minimize the effect of applied stress in Lamb wave based SHM systems.

2. Acoustoelastic Lamb Wave Propagation

The equations governing the propagation of small-amplitude waves in pre-stressed plates are briefly reviewed, following the work of Mohabuth et al. [40]. These authors used the theory of small deformations superimposed on a large deformation [39] to derive dispersion equations for Lamb wave propagation along a principal direction in a plate subjected to uniaxial stress. This framework is extended to consider the propagation of Lamb waves along a non-principal direction in a plate subjected to biaxial stresses.

Consider an isotropic plate of density ρ_0 and thickness h_0 in a stress-free reference configuration. Suppose biaxial stresses are applied in the plane of the plate such that its density and thickness change to ρ and h respectively. The deformed configuration is shown in figure 1, where the biaxial stresses σ_1 and σ_2 are assumed to be applied along the x_1 and x_2 directions of a Cartesian coordinate system $x_i = (x_1, x_2, x_3)$. The propagation of small-amplitude plane waves at an arbitrary azimuthal angle ϕ to the x_1 direction is considered.

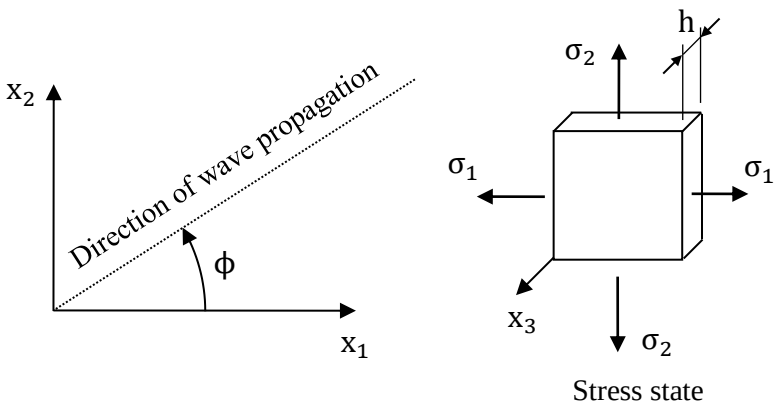

Figure 1. An infinite plate of thickness, h, subjected to biaxial loading.

The equation of motion in the pre-stressed plate and the corresponding constitutive equation are given by

$$\mathcal{A}_{piqj}\,\frac{\partial^2 u_j}{\partial x_p\,\partial x_q} = \rho\,\frac{\partial^2 u_i}{\partial t^2}, \tag{1}$$

and

$$\hat{S}_{pi} = \mathcal{A}_{piqj} \frac{\partial u_j}{\partial x_q}, \tag{2}$$

respectively, where $\boldsymbol{\mathcal{A}_0}$ is the fourth-order tensor of instantaneous elastic moduli, $\mathbf{u}$ is the incremental displacement vector associated with the wave, t is the time and $\hat{\mathbf{S}}$ is the incremental nominal stress tensor. For brevity, the derivation of the above equations is not shown here but we refer to [39] for further details.

In the present work, the elasticity tensor is expressed in terms of a third-order expanded strain energy function due to Murnaghan [41]. This form of the strain energy function is commonly used to evaluate the acoustoelastic effect in engineering materials subjected to a small pre-stress. The elasticity tensor can be obtained to the first order in the strain as

$$\begin{aligned} J\mathcal{A}_{piqj} = {} & \mu\left(\delta_{ij}\delta_{pq} + \delta_{iq}\delta_{jp}\right) + \lambda\delta_{ip}\delta_{jq} + 2\mu\left(2\delta_{ij}E_{pq} + \delta_{pq}E_{ij} + \delta_{iq}E_{jp} + \delta_{jp}E_{iq}\right) \\ & + \lambda\left(E\delta_{ij}\delta_{pq} + 2\delta_{ip}E_{jq} + 2\delta_{jq}E_{ip}\right) + 2lE\delta_{ip}\delta_{jq} \\ & + m\left[E\left(\delta_{ij}\delta_{pq} + \delta_{iq}\delta_{jp} - 2\delta_{ip}\delta_{jq}\right) + 2\left(\delta_{ip}E_{jq} + \delta_{jq}E_{ip}\right)\right] \\ & + \frac{1}{2}n\left[\delta_{ij}E_{pq} + \delta_{pq}E_{ij} + \delta_{iq}E_{jp} + \delta_{jp}E_{iq} - 2\delta_{ip}E_{jq} - 2\delta_{jq}E_{ip}\right. \\ & \left. - E\left(\delta_{ij}\delta_{pq} + \delta_{iq}\delta_{jp} - 2\delta_{ip}\delta_{jq}\right)\right], \end{aligned} \tag{3}$$

where $\mathbf{E}$ is the Green-Lagrange strain tensor, $E = \mathrm{tr}\,\mathbf{E}$, $J = 1 + E$, λ and μ are the classical Lamé elastic constants and l, m, n are the third-order elastic constants. For a given biaxial stress field defined by σ_1 and σ_2 (with $\sigma_3 = 0$), the components of $\mathbf{E}$ can simply be evaluated by means of the linear theory.

Since the wave propagation is assumed to be along a non-principal direction, the analysis is conducted in a transformed coordinate system $x_i' = (x_1', x_2', x_3')$ formed by a rotation of the x_1 and x_2 axes about the x_3 axis through the angle ϕ. The equation of motion (1) and the constitutive equation (2) then transform to

$$\mathcal{A}'_{piqj} \frac{\partial^2 u_j'}{\partial x_p' \partial x_q'} = \rho \frac{\partial^2 u_i'}{\partial t^2}, \tag{4}$$

and

$$\hat{S}'_{pi} = \mathcal{A}'_{piqj} \frac{\partial u_j'}{\partial x_q'}, \tag{5}$$

where all the quantities are now expressed in terms of the rotated coordinate system. We note that the elasticity tensor in the rotated coordinate system is related to the elasticity tensor in the original coordinate system via the tensor transformation

$$\mathcal{A}'_{piqj} = \beta_{pr}\beta_{ik}\beta_{qs}\beta_{jl}\mathcal{A}_{rksl}\,, \tag{6}$$

where β_{ij} is the cosine of the angle between x'_i and x_j.

The derivation of dispersion equations for Acoustoelastic Lamb wave propagation requires the equation of motion (4) to be solved in conjunction with stress-free boundary conditions at the surfaces of the pre-stressed plate, i.e. $\hat{S}'_{31} = \hat{S}'_{32} = \hat{S}'_{33} = 0$ at $x'_3 = \pm h/2$. Following the approach of Nayfeh and Chimenti [42], we consider solutions in the form of plane waves propagating along the x_1 direction

$$u'_j = U_j e^{i\xi(x'_1 + \alpha x'_3 - ct)}\,, \tag{7}$$

where U_j is the amplitude of the displacement, ξ is the wavenumber along the x'_1 direction, α is the ratio of the wavenumbers in the x'_3 direction to that in the x'_1 direction and c is the phase velocity in the x'_1 direction.

The detailed solution process is rather lengthy and only the final dispersion equations are presented here for reference. These are given by

$$\begin{aligned} D_{11}G_1\cot(\zeta\alpha_1) - D_{13}G_3\cot(\zeta\alpha_3) + D_{15}G_5\cot(\zeta\alpha_5) = 0\,, \\ D_{11}G_1\tan(\zeta\alpha_1) - D_{13}G_3\tan(\zeta\alpha_3) + D_{15}G_5\tan(\zeta\alpha_5) = 0\,, \end{aligned} \tag{8}$$

corresponding to the symmetric and anti-symmetric modes respectively. The definition of the various terms used in the above equations are discussed in detail in Appendix A. It is worth noting that Gandhi et al. [43] also derived similar dispersion equations. However, their analysis was performed in the natural (stress-free) coordinate system which yields the so-called natural wave velocity rather than the true wave velocity.

3. Numerical Results

The analytical equations derived can be solved numerically to obtain the phase velocity of the different guided wave modes as a function of the frequency-thickness product, the applied biaxial stress and the angle of wave propagation, i.e. $C_p(f \cdot h, \sigma_1, \sigma_2, \phi)$. The term $f \cdot h$ here refers to the product of the frequency of the wave, f and the thickness of the deformed plate, h, and the other variables are indicated in figure 1. In considering the acoustoelastic effect, it is the change in phase velocity from the unstressed state which is of interest. It is given by

$$\Delta C_p(fh_0, \sigma_1, \sigma_2, \phi) = C_p(f \cdot h, \sigma_1, \sigma_2, \phi) - C_p(f \cdot h_0, 0, 0, 0)\,, \tag{9}$$

where $C_p(f \cdot h_0, 0, 0, 0)$ refers to the unstressed phase velocity. The latter is evaluated at a frequency-thickness product $f \cdot h_0$, where h_0 corresponds to the thickness of the undeformed plate.

Dispersion results for different loads and directions of wave propagation are not discussed in detail here. These will be the subject of a later paper but we refer to the article by Gandhi et al. [43] for an overview of typical dispersion results. Although these authors conducted their analysis in the natural or unstressed coordinate system, the results are qualitatively the same as in the case of the deformed coordinate system. In the present paper, we focus on the fundamental symmetric (S0) and anti-symmetric (A0) modes due to their relevance in SHM applications. The material considered is 6061-T6 Aluminium and its elastic properties are summarised in Table 1.

Table 1. Elastic Properties of 6061-T6 Aluminium

Parameter	Aluminium[44]
$\boldsymbol{\lambda}$ **[GPa]**	54.308
$\boldsymbol{\mu}$ **[GPa]**	27.174
l [GPa]	−281.5
m [GPa]	−339.0
n [GPa]	−416.0
$\boldsymbol{\rho}$ **[kg/m^3]**	2704
$\boldsymbol{\sigma_y}$ **[MPa]**	300

Note: The yield strength, σ_y , was not mentioned in [44]; thus an average of the typical values for this material is given in Table 1.

Figure 2 shows the change in the phase velocity of the fundamental Lamb wave modes for a plate subjected to a range of uniaxial strains (stresses). The waves are considered to be propagating along the direction of the applied load such that $\phi = 0^o$. It can be seen that at any given frequency-thickness product, the magnitude of the change in the phase velocity is directly proportional to the applied stress (strain) for both the A0 and S0 modes. In the case of the A0 mode, an interesting behaviour can be observed at a frequency-thickness product of approximately 350 Hz-m. As shown in the insert plot in figure 2(a), the change in the phase velocity of the A0 mode is zero at this frequency-thickness product. This particular frequency does not seem to be dependent on the magnitude of the applied strain (stress) as previously reported by Mohabuth et al. [40].

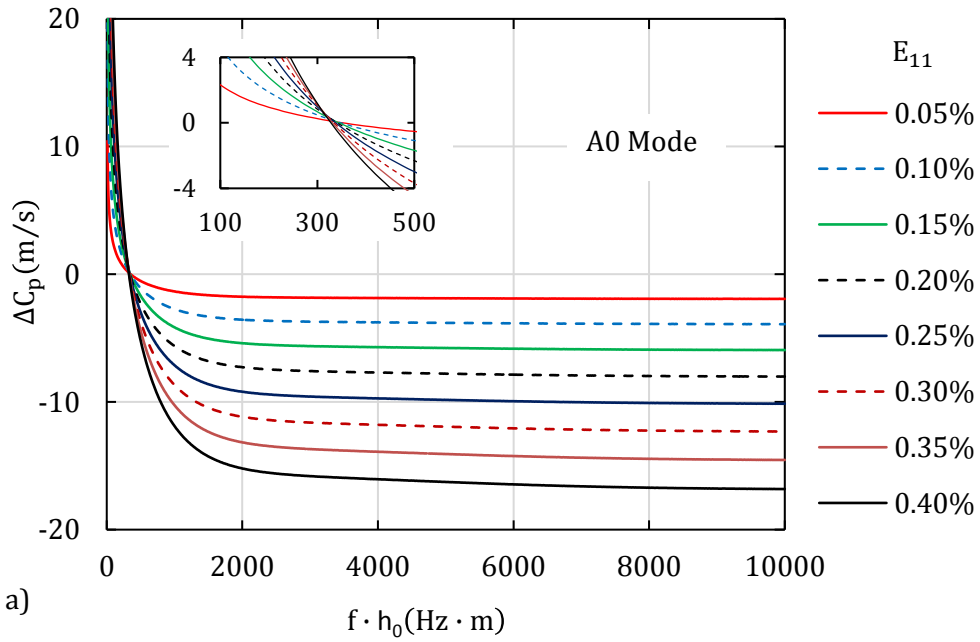

a)

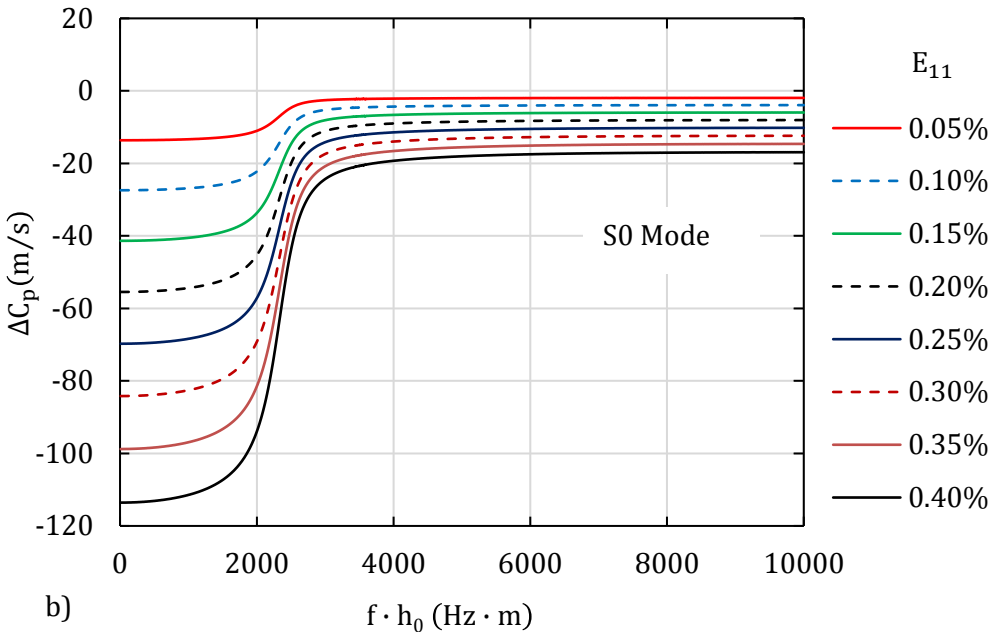

Figure 2. Effect of strain (stress) on the change in phase velocity of the fundamental Lamb wave modes, a) A0 Mode and b) S0 Mode, propagating along the direction of the applied strain (stress).

Figure 3 shows the change in the phase velocity of the fundamental Lamb wave modes for a plate subjected to a uniaxial stress of 100 MPa for different angles of wave propagation. The load is applied along the x_1 axis such that waves propagating parallel to the applied load are at $\phi = 0^o$. Due to the strain induced anisotropy, the change in the phase velocity is dependent on the direction of wave propagation. Considering the A0 mode, there is a critical frequency-thickness product (f_{Cr}) of approximately 300 Hz-m at which ΔC_p is invariant of the angle of wave propagation. As shown in the insert plot in figure 3 (a), the magnitude of ΔC_p at this particular frequency is small but non-zero. This phenomenon was also pointed out by Gandhi et al. [43]. At frequencies below f_{Cr}, the magnitude of ΔC_p is lowest when the wave propagation is perpendicular to the applied stress. At higher frequencies, it can be seen that the curves corresponding to $\phi < 60^o$ intercept the horizontal axis ($\Delta C_p = 0$) at different frequencies. These combinations of wave propagation angles and zero-intercept frequencies may be used in the development of stress mitigation strategies. These will be discussed in detail in Section 5.

In the case of the S0 mode, the curves for wave propagation at an oblique angle to the applied stress are not drawn beyond a certain threshold frequency-thickness product (f_{Th}) of 3400 Hz-m. This is because at this frequency, the S0 mode and the fundamental shear-horizontal (SH0) mode interact

with each other, split and propagate as two hybridised modes. This behaviour was also reported by Gandhi et al. [43]. For wave propagation at $\phi = 0^0$ or 90^0, this behaviour does not occur as the direction of wave propagation is aligned with the principal axes and therefore, the motion of the S0 and SH0 modes are decoupled.

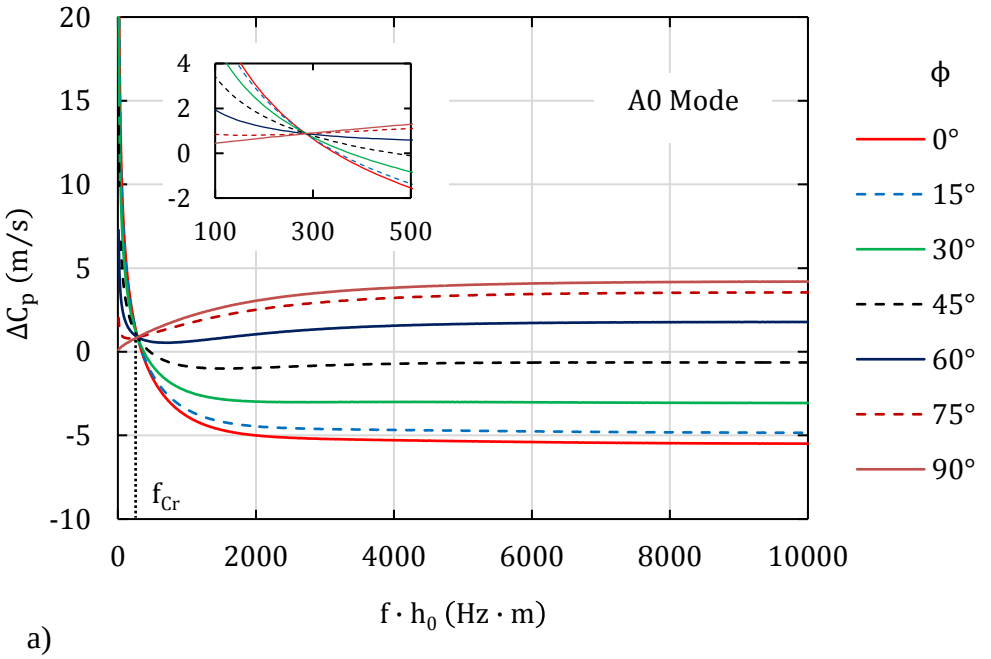

a)

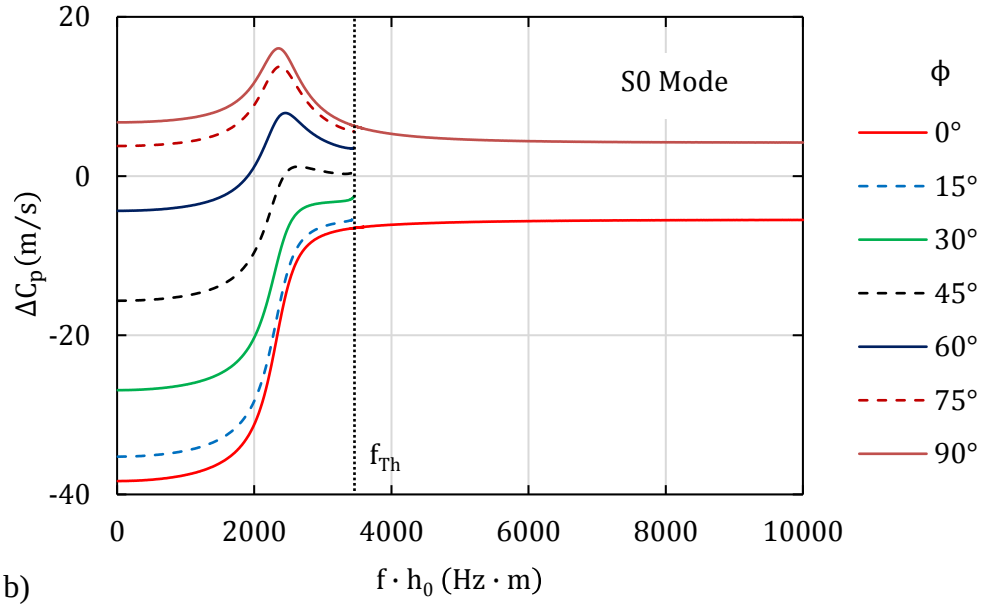

b)

Figure 3. Change in the phase velocity of the fundamental Lamb wave modes: a) A0 mode and b) S0 mode in a plate subjected to a uniaxial stress of $\sigma_1 = 100$ MPa (the stress acts along direction $\phi = 0^o$, see Fig.1).

The change in phase velocity for a biaxial stress field can also be evaluated from the Taylor expansion of equation (9) utilising the change in phase velocity due to the two uniaxial contributions. This can be written as

$$\Delta C_p(f \cdot h_0, \sigma_1, \sigma_2, \phi) \approx K_{\sigma_1}\sigma_1 + K_{\sigma_2}\sigma_2 \,, \tag{10}$$

where K_{σ_1} and K_{σ_2} are the coefficients relating changes in the phase velocity due to the uniaxial stresses σ_1 and σ_2 respectively. These are given by

$$K_{\sigma_1} \approx \left.\frac{\partial C_p}{\partial \sigma_1}\right|_{(f\cdot h_0, \sigma_1, 0, \phi)} \approx \frac{C_p(f \cdot h_1, \sigma_1, 0, \phi) - C_p(f \cdot h_0, 0, 0, 0)}{\sigma_1 - 0}, \tag{11}$$

$$K_{\sigma_2} \approx \left.\frac{\partial C_p}{\partial \sigma_2}\right|_{(f\cdot h_0, 0, \sigma_2, \phi)} \approx \frac{C_p(f \cdot h_2, 0, \sigma_2, \phi) - C_p(f \cdot h_0, 0, 0, 0)}{\sigma_2 - 0}, \tag{12}$$

where h_1 and h_2 correspond to the thicknesses of the deformed plate due to the uniaxial stresses σ_1 and σ_2 respectively.

Equation (10) provides a very convenient approximation to compensate for load effects in practice. It was validated via direct numerical simulations for both the S0 and A0 modes. The validation process was carried out as follows: (i) the change in phase velocity was evaluated for a range of uniaxial stresses and angles of wave propagation; (ii) the coefficients K_{σ_1} and K_{σ_2} were then calculated from the ratio of the change in phase velocity to the uniaxial stress based on equations (11) and (12); (iii) the analytical equations (8) were numerically solved for different biaxial stresses and directions of wave propagation; (iv) the coefficients K_{σ_1} and K_{σ_2} evaluated in (ii) were substituted in equation (10) to approximate the change in the phase velocity predicted by the analytical equations in (iii).

Figure 4 shows the variation of the coefficient K_{σ_1} as a function of the frequency-thickness product for the A0 and S0 modes for a range of applied strains (stresses). The waves are considered to be along the direction of the applied strain. The results show that K_{σ_1} does not have any significant dependence on the magnitude of the applied strain. This finding is consistent with the results of

Gandhi et al. [43] who demonstrated that the change in the phase velocity is linear with load for a small pre-stress. Thus, in the remainder of the paper, K_{σ_1} will be considered to be only a function of the frequency-thickness product and the angle of wave propagation. For completeness, the variation of K_{σ_1} at different angles of wave propagation are shown in Appendix B. The variation of the coefficient K_{σ_2} is not shown as it may be evaluated from its σ_1 counterpart using the relation $K_{\sigma_2}(f \cdot h_0, \phi) \equiv K_{\sigma_1}(f \cdot h_0, 90^o - \phi)$.

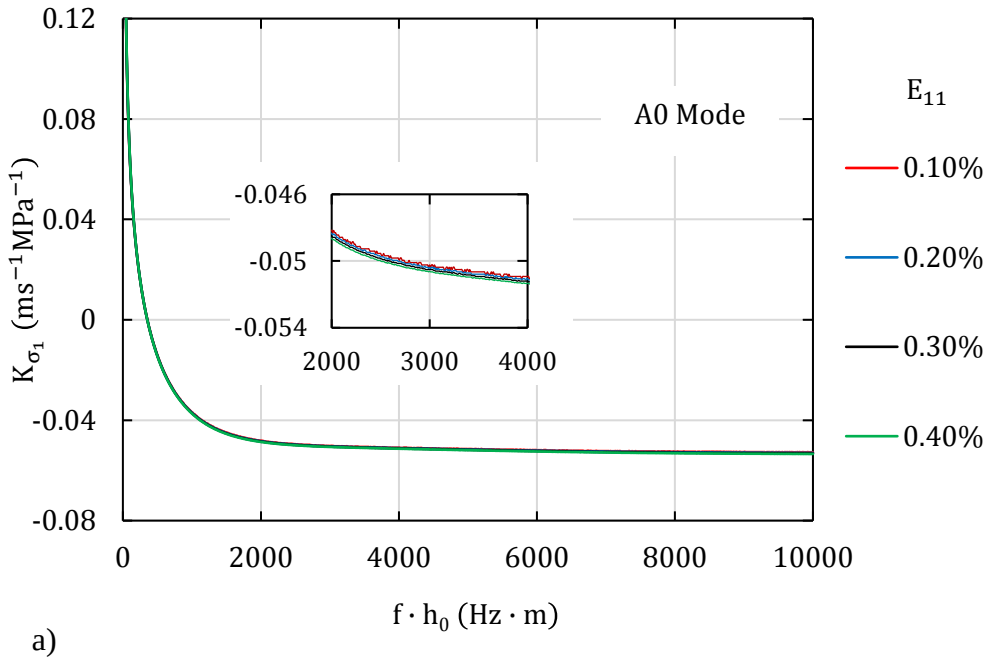

a)

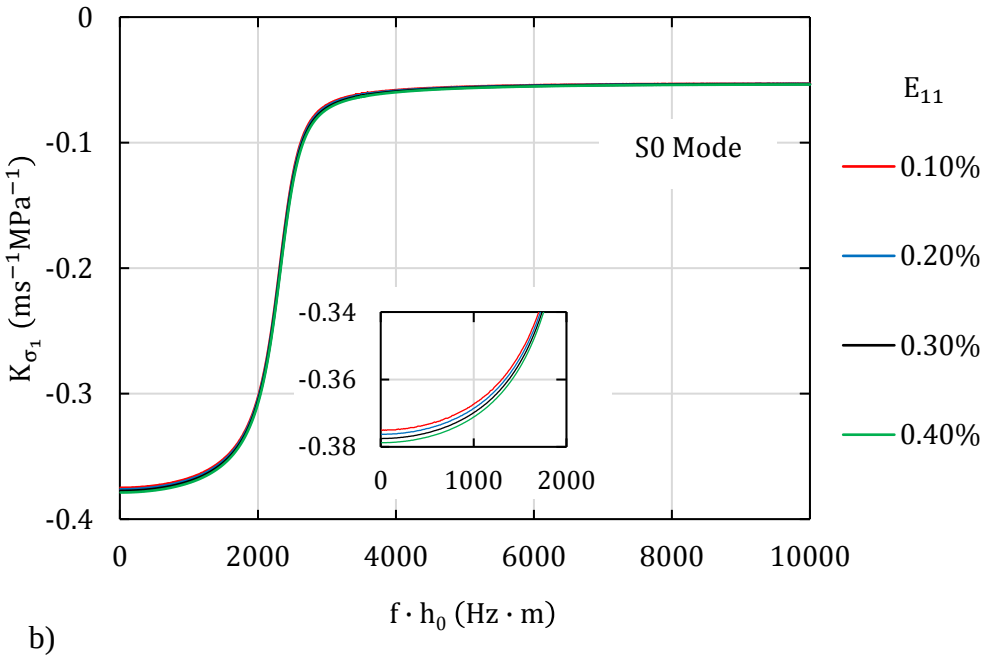

b)

Figure 4. Effect of strain (stress) on the coefficient relating changes in C_p to the applied stress σ_1 for the (a) A0 mode and, (b) S0 mode, propagating along the direction of the applied strain (stress).

The results obtained using the representation (10), along with the values of K_{σ_1} and K_{σ_2} from Appendix B, were found to be in good agreement with the phase velocity changes predicted by the analytical equations (8) for all cases considered. The root mean square (RMS) differences between the two models for a typical case corresponding to $\sigma_1 = 100$ MPa and $\sigma_2 = 50$ MPa are shown in Table 2. The highest RMS difference for the A0 and S0 modes are 0.030 m/s and 0.099 m/s respectively; these relatively small values are representative of all the cases considered. Thus, the approximation in equation (10) may be assumed to be correct. Shi et al. [45] proposed similar equations to estimate the change in phase velocity for various biaxial loads and propagation directions. Although their analysis was conducted in the undeformed (natural) coordinate system, their results also demonstrate the feasibility of estimating the phase velocity changes for a biaxial stress field based on the linear combination of the change in phase velocity due to the uniaxial loads.

Table 2. Root mean square differences between the analytical and approximate models

	RMS difference (m/s)	
ϕ	A0 Mode	S0 Mode
0º	0.030	0.078
30º	0.014	0.096
45º	0.030	0.071
60º	0.013	0.099
90º	0.029	0.069

4. Stress Effect on Damage Diagnostic with guided waves

In this section, an analytical model is presented to quantify the residual signal (noise) obtained after reference signal subtraction due to the effect of applied (biaxial) stress. Two different methods of signal subtraction can be utilised in SHM systems. These methods can be based on either the shift in the envelope of the wave packet or on the shift of the individual waves in the wave packet respectively. Although the envelope subtraction method led to an improved sensitivity to damage, it was demonstrated that this particular method can result in areas where damage detection is not possible due to the loss of phase information in the enveloping process [28]. Therefore, the focus of this paper will be on the evaluation of the shift of the individual waves in the wave packet due to applied stress, which seems to be a more robust technique for damage diagnostics using GW.

Following the work of Croxford et al. [28], the reference signal is considered to be a Hanning-windowed toneburst, which is widely utilised in GW based SHM applications. It was demonstrated that in the presence of temperature variations, δT, the algebraic signal subtraction of the time trace affected by temperature from the reference data results in the following expression for the residual signal or noise:

$$u_{noise} = 2u_0 \pi f \frac{d}{C_p}\left(\alpha - \frac{K_T}{C_p}\right)\delta T\,, \tag{13}$$

where u_0 is the amplitude of the received signal, f is the centre frequency of the toneburst, d is the propagation distance between the transmitting and receiving transducers, C_p is the phase velocity of the wave, α is the coefficient of thermal expansion of the material and K_T is the coefficient relating changes in C_p to temperature.

Similar to the effect of temperature variations on GW propagation, a change in the stress state of a structure also leads to a translation in time of the received signal. This is because the applied stress not only causes a change in the wave propagation distance due to the induced strain but also leads to a change in the phase velocity due to the strain induced anisotropy. In order to establish a relationship between the change in the arrival time of the received signal, δt, and the change in the stress state of the structure, characterised by $\delta\sigma_1$ and $\delta\sigma_2$, we start from $t = \frac{d}{C_p}$ and take partial derivatives with respect to d and C_p, which gives

$$\delta t = \frac{1}{C_p}\left(\frac{\delta d}{\delta\sigma_1}.\delta\sigma_1 + \frac{\delta d}{\delta\sigma_2}.\delta\sigma_2\right) - \frac{d}{{C_p}^2}\left(\frac{\delta C_p}{\delta\sigma_1}.\delta\sigma_1 + \frac{\delta C_p}{\delta\sigma_2}.\delta\sigma_2\right). \tag{14}$$

If the pre-deformation (from a stress-free reference configuration) is considered to be small, the relationship between the propagation distance and the applied stress can be expressed using Generalised Hooke's law as

$$\begin{aligned} \frac{\delta d}{\delta\sigma_1} &= \frac{d}{2E_Y}[1 - \nu + (1+\nu)\cos(2\phi)] = \beta_1(\phi)d, \\ \frac{\delta d}{\delta\sigma_2} &= \frac{d}{2E_Y}[1 - \nu - (1+\nu)\cos(2\phi)] = \beta_2(\phi)d, \end{aligned} \tag{15}$$

where E_Y is the Young's modulus of the material, ν is the Poisson's ratio and ϕ is the angle of wave propagation (measured relative to the σ_1 axis). The relationship between the wave velocity and the applied stress can be written as

$$\frac{\delta C_p}{\delta\sigma_1} = K_{\sigma_1}(f\cdot h_0, \phi), \qquad \frac{\delta C_p}{\delta\sigma_2} = K_{\sigma_2}(f\cdot h_0, \phi)\,, \tag{16}$$

where K_{σ_1} and K_{σ_2} are the coefficients relating changes in C_p to the uniaxial stresses σ_1 and σ_2 respectively, as defined by equation (10). These coefficients may be evaluated based on the acoustoelastic model described earlier in the paper. They are functions of the frequency-thickness product, $f\cdot h_0$, due to the dispersive nature of guided waves and the angle of wave propagation, ϕ (measured relative to the σ_1 axis). Substituting equations (15) and (16) into equation (14) leads to an expression for δt in terms of $\delta\sigma_1$

$$\delta t = \frac{d}{C_p}\left[(\beta_1 + \beta_2\lambda) - \frac{\left(K_{\sigma_1} + K_{\sigma_2}\lambda\right)}{C_p}\right]\delta\sigma_1 , \tag{17}$$

where $\lambda = \delta\sigma_2/\delta\sigma_1$ is the biaxial stress ratio.

Assuming that δt is sufficiently small, the noise can be approximated as

$$u_{noise} = 2u_0\pi f\delta t . \tag{18}$$

Finally, combining equation (17) with equation (18) gives

$$u_{noise} = 2u_0\pi f\frac{d}{C_p}\left[(\beta_1 + \beta_2\lambda) - \frac{\left(K_{\sigma_1} + K_{\sigma_2}\lambda\right)}{C_p}\right]\delta\sigma_1 . \tag{19}$$

In general, the magnitudes of K_{σ_1}/C_p and K_{σ_2}/C_p are of the same order as those of β_1 and β_2; so both the change in propagation distance d due to the induced strain and the change in C_p due to the strain induced anisotropy should be considered. However, in the case of thermally induced stress, β_1 and β_2 should be set to zero as the propagation distance remains unchanged.

Both equations (13) and (19) indicate that the noise associated with changing temperature or stress is dependent on the distance between the transmitting and receiving transducers. Thus, if the signal-to-noise ratio is known, the maximum propagation distance or the minimum density of the sensor/transmitter array can be evaluated. These equations also suggest that faster guided wave modes with higher phase velocities are less affected by changes in temperature or stress as compared to slower modes. However, faster modes typically propagate at relatively high frequencies and, as a result, there is a trade-off between frequency and phase velocity as the noise is directly proportional to f but is inversely proportional to C_p. In general, lower frequencies are preferred for SHM applications as the number of modes propagating in the waveguide is minimized, thus making the signal analysis less complex.

Example

The effect of stress on the residual noise is significant and is in fact comparable to the effect of temperature. To demonstrate this point, let us consider a 1 mm thick 6061-T6 Aluminium plate in a stress free state at a reference temperature, T_0. If the in-plane edges of the plate are constrained, a uniform temperature rise of 1 ^{o}C will induce compressive biaxial stresses of approximately $\sigma_1 = \sigma_2 = -E\alpha/(1-v) \times 1\ ^{o}C \approx -2.56$ MPa. To quantify the effect of temperature and the thermally

induced stress, an excitation signal with a centre frequency of 1 MHz is employed and the direction of wave propagation is chosen to be parallel to the σ_1 direction.

Table 3. Temperature and stress coefficients for a 6061-T6 Aluminium plate at a frequency-thickness product of 1 MHz − mm and an angle of wave propagation of 0^o.

	A0	**S0**
$\mathbf{K_T\ (ms^{-1}\ ^oC^{-1})}$	-0.383	-1.237
$\mathbf{K_{\sigma_1}\ (ms^{-1}MPa^{-1})}$	-0.037	-0.371
$\mathbf{K_{\sigma_2}\ (ms^{-1}MPa^{-1})}$	0.021	0.073

Table 3. summarises the values of the temperature and stress coefficients, K_T, K_{σ_1} and K_{σ_2}, at the corresponding frequency-thickness product for the fundamental Lamb wave modes. The temperature coefficients were extracted using the same approach as in Croxford et al. [28]; the material properties of 6061-T6 Aluminium were used along with $\alpha = 23.6 \times 10^{-6}\ ^oC^{-1}$, $k_S = -0.752\ ms^{-1}\ ^oC^{-1}$ and $k_L = -1.089\ ms^{-1}\ ^oC^{-1}$, where k_S and k_L are the temperature dependence constants for shear and longitudinal wave speeds respectively. The stress coefficients K_{σ_1} and K_{σ_2} were extracted from Appendix B at an angle of propagation of 0^o and 90^o respectively. The effect of temperature on the material properties is not considered while evaluating these stress coefficients.

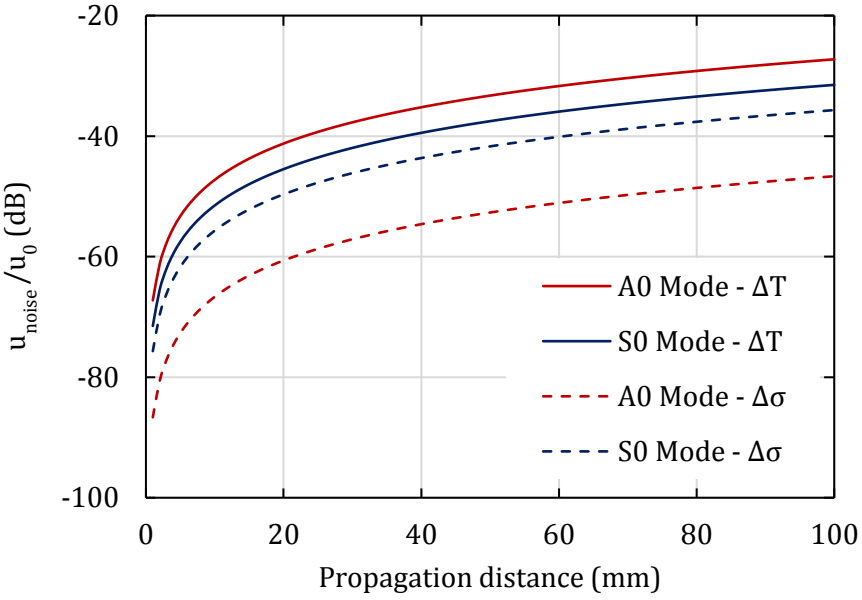

Figure 5. Variation of u_{noise}/u_0 with the propagation distance for the fundamental Lamb wave modes in an Aluminium plate at a frequency-thickness product of 1 MHz − mm. The solid lines represent the noise due to a 1 ^oC temperature change while the dotted lines represent the noise associated with the induced (biaxial) thermal stress in a plate constrained at its in-plane edges.

The coefficients in Table 3 were then substituted in equations (13) and (19) to predict the noise due to a temperature change of 1 ^oC as well as the noise associated with the induced (compressive biaxial) thermal stress. The coefficients α, β_1 and β_2 in the latter equations were set to zero as the propagation distance remains unchanged in the constrained plate. The results are presented in terms of the ratio u_{noise}/u_0 as a function of the propagation distance for the fundamental Lamb wave modes, as shown in figure 5. It can be seen that the noise is more sensitive to the change in temperature as compared to the thermally induced stress. This is not unexpected as the magnitude of K_T is higher than those of K_{σ_1} and K_{σ_2}. It can also be seen that the A0 mode is more affected by the change in temperature than the S0 mode. Croxford et al. [28] attributed this behaviour to the effect of the higher phase velocity of the S0 mode which reduces its sensitivity to temperature. However, in the case of thermally induced stress, this effect is largely mitigated as the stress coefficient K_{σ_1} for the S0 mode is an order of magnitude higher than that of the A0 mode. As a result, the S0 mode exhibits a much larger sensitivity to the thermally induced stress than the A0 mode.

It is interesting to note that in a constrained plate, the thermally induced stress might partially compensate for the effect of temperature on the phase velocity and the associated noise generation. This is because the temperature change and the thermally induced stress usually have an opposite effect on the phase velocity of the fundamental Lamb wave modes. For example, at a frequency-thickness of 1 MHz − mm and an angle of propagation parallel to the σ_1 direction, a positive change in temperature ($\delta T > 0$) leads to a decrease in the phase velocity whereas the induced (compressive) thermal stress ($\delta\sigma_1, \delta\sigma_2 < 0$) causes an increase in the phase velocity. Consequently, the stress effect partially compensates for the effect of temperature on the phase velocity and the associated noise generation. However, this is not always the case as the change in the phase velocity depends on the magnitude and sign of the temperature and stress coefficients. The latter coefficients are both functions of the signal frequency while the stress coefficients also have an additional dependence on the angle of wave propagation.

5. Possible stress mitigation strategies

The behaviour of the A0 mode demonstrates some interesting features, which can potentially be utilised for future stress mitigation techniques. In particular, the results presented earlier show the existence of a critical frequency-thickness product, f_{Cr}, at which the phase velocity is invariant of the direction of wave propagation, ϕ. This frequency does not appear to be affected by the magnitude of the applied stress. Although the change in the phase velocity from the unstressed state is non-zero at this critical frequency, its magnitude is relatively small. Therefore, in the case where the Lamb wave toneburst is dominated by the A0 mode and the direction of the applied load is unknown, the influence of the applied stress can be minimized by selecting a frequency close to f_{Cr} at which the values of the stress coefficients, K_{σ_1} and K_{σ_2}, tend to zero.

In practical systems, the excitation signal is typically generated using piezo-ceramic transducers and this causes the signal to have a finite bandwidth. Since the critical frequency f_{Cr} is within the dispersive region of the A0 mode, a large bandwidth may affect the implementation of the above strategy. Windowing techniques such as Hanning window may be used to reduce the bandwidth and ensure that the energy of the signal is concentrated near the central excitation frequency. Although a narrower bandwidth will reduce the problem of dispersion, post processing techniques [46-48] may still be required to compensate for the effect of dispersion.

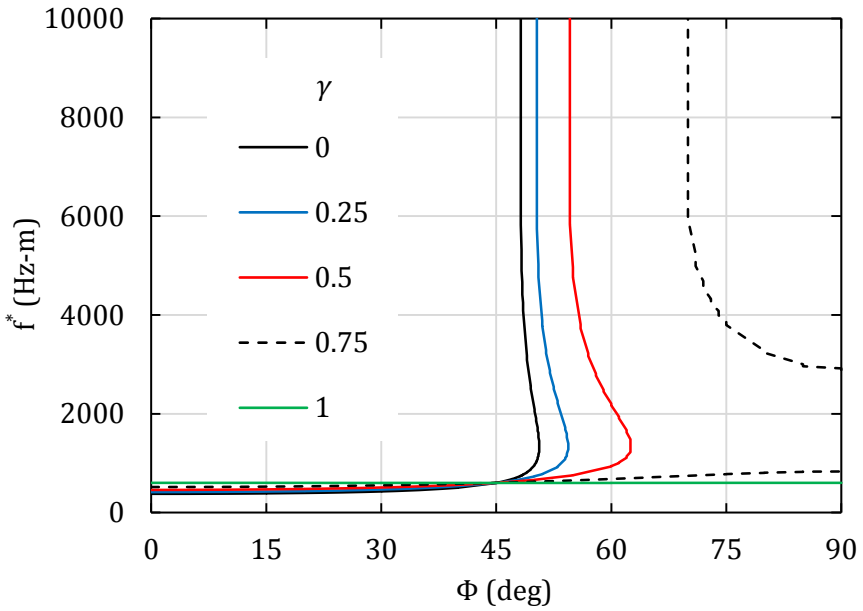

Figure 6. Variation of the zero-intercept frequency, f^*, for the A0 mode as a function of the angle of wave propagation, ϕ, for different biaxial stress ratios, λ, with σ_1= 20 MPa.

A more accurate stress mitigation technique may be employed if the direction of the applied load is known. This involves using the frequency at which the change in the phase velocity of the A0 mode from the unstressed state is zero. Figure 6 displays the variation of this zero-intercept frequency, f^*, as a function of the angle of wave propagation for different biaxial stress ratios. The magnitude of the first principal stress, σ_1, is kept constant at 20 MPa. The results indicate that the optimum orientation of transducers is at an angle of 45 degrees to the principal axes. At this angle, the corresponding zero-intercept frequency is independent of the biaxial stress ratio. In addition, the latter frequency only shows a weak dependence on the magnitude of the applied stress σ_1. It can be hypothesised that a similar behaviour also occurs for other materials. In practice, guided wave based SHM schemes typically utilise an omni-directional transducer array as they rely on multi-directional propagation to achieve full coverage of a structure [49-50]. The transducers in the array are at varying pre-defined angles to each other. In this case, the effect of the applied stress can be effectively negated by selecting an excitation frequency equal to the zero-intercept frequency for the specific angle between two selected transducers.

For certain guided wave based SHM applications, the S0 mode may be preferred over the A0 mode. In this case, the viable strategy in the reduction of the residual noise due to stress variations would be the utilisation of frequency-thickness products, below the threshold frequency shown in figure 3(b). The effect of stress on the change in the phase velocity decreases significantly as we approach this particular frequency. The use of the S0 mode above this threshold frequency-thickness should be avoided due to the complexities associated with mode splitting.

6. Conclusion

In this paper, the effect of stresses on the propagation of Lamb waves was analysed using an acoustoelastic formulation to determine the change in the phase velocity as a function of the applied stress, frequency and propagation direction. An analytical model was then developed to assess the residual signal or noise due to applied or thermally-induced stresses. It was demonstrated that the effect of stresses can be as strong as the effect of temperature fluctuations, and it has to be considered when implementing guided wave based SHM systems in real-world applications.

It was interesting to find that applied stresses have a very different influence on the phase velocity of the fundamental symmetric and anti-symmetric modes. In particular, for the S0 mode, as we approach a certain threshold frequency, the effect of stress on the change in the phase velocity decreases significantly. In the case of the A0 mode, there is a critical value of frequency at which the

influence of stress on the change in the phase velocity is almost negligible. These features can be utilised in the development of effective stress mitigation strategies for on-line SHM systems.

This paper has considered a particular case of a plate made of Aluminium to demonstrate the importance of the stress effect on noise generation after reference signal subtraction. It should be emphasised that any variability in the material properties of the plate, especially in the third order elastic constants, will lead to a change in the magnitude of the phase velocity dispersion curves. While it is expected that general trends and outcomes of the paper will be qualitatively the same, it would be beneficial to conduct a thorough quantitative analysis in the future.

Acknowledgement

The work was supported by the Australian Government Research Training Program Scholarship, and the Australian Research Council, project DP160102233.

References

[1] Maalej M, Karasaridis A, Pantazopoulou S and Hatzinakos D 2002 Structural health monitoring of smart structures *Smart Mater. Struct.* **11** 581-589

[2] Su Z and Ye L 2009 *Identification of damage using Lamb waves: from fundamentals to applications* ed F Pfeiffer and P Wriggers (Berlin: Springer)

[3] Staszewski W, Boller C and Tomlinson G R 2004 Health Monitoring of Aerospace Structures: Smart Sensor Technologies and Signal Processing (Chichester: John Wiley & Sons)

[4] Staszewski W J 2004 Structural Health Monitoring Using Guided Ultrasonic Waves *Advances in Smart Technologies in Structural Engineering* ed J Holnicki-Szulc and C A Mota Soares (Berlin: Springer) pp 117–162

[5] Su Z, Ye L and Lu Y 2006 Guided Lamb waves for identification of damage in composite structures: a review *J. Sound Vib*. **295** 753–80

[6] Park G, Farrar C R, Lanza di Scalea F and Coccia S 2006 Performance assessment and validation of piezoelectric active-sensors in structural health monitoring *Smart Mater. Struct*. **15** 1673-1683.

[7] Raghavan A and Cesnik C E S 2007 Review of Guided-wave Structural Health Monitoring *The Shock Vib. Dig.* **39** 91-114

[8] Mitra M and Gopalakrishnan S. 2016 Guided wave based structural health monitoring: A review *Smart Mater. Struct*. **25** 053001

[9] Giurgiutiu V 2016 Structural Heal Monitoring of Aerospace Composites (London: Academic Press)

[10] Michaels J E 2008 Detection, localization and characterization of damage in plates with an in situ array of spatially distributed ultrasonic sensors *Smart Mater. Struct*. **17** 1-15

[11] Zak A, Radzienski M, Krawczuk M, Ostachowicz W 2012 Damage detection strategies based on propagation of guided elastic waves *Smart Mater. Struct*. **21** 035024

[12] He S and Ng C T. 2016 A probabilistic approach for quantitative identification of multiple delaminations in laminated composite beams using guided waves *Eng. Struct.* **127** 602-614

[13] He S and Ng C T. 2017 Guided wave-based identification of multiple cracks in beams using a Bayesian approach *Mech. Syst Sig. Process.* **84** 324-345

[14] Staszewski W J 2005 Ultrasonic/Guided Waves for Structural Health Monitoring *Key Eng. Mat.* **293-294** 49-62

[15] Schmidt D, Hillger W, Szewieczek A and Sinapius M 2013 Structural Health Monitoring Based on Guided Waves *Adaptive, tolerant and efficient composite structures* (Heidelberg: Springer) pp 449-462

[16] Diamanti K and Soutis C 2010 Structural health monitoring techniques for aircraft composite structures *Prog. Aerosp. Sci.* **46** 342-352

[17] Konstantinidis G, Drinkwater B W and Wilcox P D 2006 The temperature stability of guided wave structural health monitoring systems. *Smart Mater. Struct.* **15** 967-976

[18] Lanza di Scalea F and Salamone S 2008 Temperature effects in ultrasonic Lamb wave structural health monitoring systems *J. Acoust. Soc. Am.* **124** 161-174

[19] Raghavan A and Cesnik C E S 2008 Effects of Elevated temperature on Guided-wave Structural Health Monitoring *J. Intel. Mat. Sys. Struct.* **19** 1383-1398

[20] Dodson J C and Inman D J 2013 Thermal sensitivity of Lamb waves for structural health monitoring applications *Ultrasonics* **53** 677-685

[21] Dodson J C and Inman D J 2014 Investigating the thermally induced acoustoelastic effect in isotropic media with Lamb waves *J. Acoust. Soc. Am.* **136** 2532-2543

[22] Chen F and Wilcox P D 2007 The effect of load on guided wave propagation *Ultrasonics* **47** 111-122

[23] Sohn H 2007 Effects of environmental and operational variability on structural health monitoring *Phil. Trans. R. Soc. A* **365** 539–60

[24] Michaels J E, Michaels T E and Martin R S 2009 Analysis of global ultrasonic sensor data from a full scale wing panel test *AIP Conference Proceedings* **1096** 950-957

[25] Lee S J, Gandhi N, Michaels J E and Michaels T E 2011 Comparison of the effects of applied loads and temperature variations on guided wave propagation *AIP Conference Proceedings* **1335** 175-182

[26] Michaels J E, Gandhi N and Lee S J 2011 Acoustoelastic Lamb Waves and Implications for Structural Health Monitoring *From Waves in Complex Systems to Dynamics of Generalized Continua* ed K Hutter, T T Wu and Y C Shu (New Jersey: World Scientific) pp 91-117

[27] Roy S, Ladpli P and Chang F-K 2015 Load monitoring and compensation strategies for guided-waves based structural health monitoring using piezoelectric transducers *J. Sound Vib* **351** 206-220

[28] Croxford A J, Wilcox P D, Drinkwater B W and Konstantinidis G 2007 Strategies for guided-wave structural health monitoring *Proc. R. Soc. A* **463** 2961–2981

[29] Aryan P, Kotousov A, Ng C T and Cazzolato B 2017 A model-based method for damage detection with guided waves *Struct. Control Health Monit.* **22** e1884

[30] Aryan P, Kotousov A, Ng C T and Wildy S 2016 Reconstruction of baseline time-trace under changing environmental and operational conditions *Smart Mater. Struct.* **25** 035018

[31] Lu Y and Michaels J E 2005 A methodology for structural health monitoring with diffuse ultrasonic waves in the presence of temperature variations *Ultrasonics* **43** 717-731

[32] Clarke T, Cawley P, Wilcox P D and Croxford A J 2009 Evaluation of the damage detection capability of a sparse-array guided-wave SHM system applied to a complex structure under varying thermal conditions *IEEE Trans. Ultrason. Ferroelect. Freq. Contr.* **56** 2666-2678

[33] Salamone S, Bartoli I, Lanza di Scalea F and Coccia S 2009 Guided–wave Health Monitoring of Aircraft Composite Panels under Changing Temperature *J. Intel. Mat. Sys. Struct.* **20** 1079-1090

[34] Clarke T, Simonetti F and Cawley P 2010 Guided wave health monitoring of complex structures by sparse-array systems: influence of temperature changes on performance *J. Sound Vib.* **329** 2306-2322

[35] An Y K and Sohn H 2010 Instantaneous crack detection under varying temperature and static loading conditions *Struct. Control Health Monit* **17** 730–741

[36] Croxford A J, Moll J, Wilcox P D and Michaels J E 2010 Efficient temperature compensation strategies for guided wave structural health monitoring *Ultrasonics* **50** 517-528

[37] Dao P B and Staszewski W J 2013 Cointegration approach for temperature effect compensation in Lamb-wave based damage detection *Smart Mater. Struct.* **22** 1-20

[38] Michaels J E 2016 Sparse array imaging with guided waves under variable environmental conditions *Structural Health Monitoring (SHM) in Aerospace Structures* (Cambridge-Woodhead Publishing) pp 255-284

[39] Ogden R W 1984 *Non-Linear Elastic Deformations* (Chichester: Ellis Horwood)

[40] Mohabuth M, Kotousov A and Ng C T 2016 Effect of uniaxial stress on the propagation of higher-order Lamb wave modes *Int. J. Nonlinear Mech.* **86** 104-111

[41] Murnaghan F D 1937 Finite Deformations of an Elastic Solid *Am. J. Math.* **59** 235-260

[42] Nayfeh A H and Chimenti D E 1989 Free Wave Propagation in Plates of General Anisotropic Media *J. Appl. Mech.* **56** 881-886

[43] Gandhi N, Michaels J E and Lee S J 2012 Acoustoelastic Lamb wave propagation in biaxially stressed plates *J. Acoust. Soc. Am.* **132** 1284-1293

[44] Asay J R and Guenther A H 1967 Ultrasonic studies of 1060 and 6061-T6 aluminum *J. Appl. Phys.* **38** 4086–4088

[45] Shi F, Michaels J E and Lee S J 2013 In situ estimation of applied biaxial loads with Lamb waves *J. Acoust. Soc. Am.* **133** 677-687

[46] Wilcox P D 2003 A Rapid Signal Processing Technique to Remove the Effect of Dispersion from Guided Wave Signals *IEEE Trans. Ultrason., Ferroelect., Freq. Contr.* **50** 419-427

[47] Zeng L, Lin J 2014 Chirp-based dispersion pre-compensation for high resolution Lamb wave inspection *NDT & E Int.* **61** 35–44

[48] Liu L and Yuan F G 2009 A linear mapping technique for dispersion removal of Lamb wave *Smart Mater. Struct.* **9** 75-86.

[49] Wilcox P D 2003 Omni-Directional Guided Wave Transducer Arrays for the Rapid Inspection of Large Areas of Plate Structures *IEEE Trans. Ultrason., Ferroelect., Freq. Contr.* **50** 699-709

[50] Koduru J P and Rose J L 2012 transducer arrays for omnidirectional guided wave mode control in plate like structures *Smart Mater. Struct.* **22** 015010

Appendix A

Following the work of Nayfeh and Chimenti [42], the plane waves solution given by equation (7) is substituted into the equation of motion (4). This yields an eigenvalue problem which can be expressed as

$$K_{ij}(\alpha)\, U_j = 0, \qquad i,j = 1,2,3 \tag{A1}$$

where

$$\begin{aligned}
K_{11} &= \rho c^2 - \mathcal{A}'_{1111} - \mathcal{A}'_{3131}\,\alpha^2 - \alpha(\mathcal{A}'_{1131} + \mathcal{A}'_{3111}),\\
K_{12} &= -\mathcal{A}'_{1112} - \mathcal{A}'_{3132}\,\alpha^2 - \alpha(\mathcal{A}'_{1132} + \mathcal{A}'_{3112}),\\
K_{13} &= -\mathcal{A}'_{1113} - \mathcal{A}'_{3133}\,\alpha^2 - \alpha(\mathcal{A}'_{1133} + \mathcal{A}'_{3113}),\\
K_{21} &= -\mathcal{A}'_{1211} - \mathcal{A}'_{3231}\,\alpha^2 - \alpha(\mathcal{A}'_{1231} + \mathcal{A}'_{3211}),\\
K_{22} &= \rho c^2 - \mathcal{A}'_{1212} - \mathcal{A}'_{3232}\,\alpha^2 - \alpha\left(\mathcal{A}'_{1232} + \mathcal{A}'_{0_{3212}}\right),\\
K_{23} &= -\mathcal{A}'_{1213} - \mathcal{A}'_{3233}\,\alpha^2 - \alpha(\mathcal{A}'_{1233} + \mathcal{A}'_{3213}),\\
K_{31} &= -\mathcal{A}'_{1311} - \mathcal{A}'_{3331}\,\alpha^2 - \alpha(\mathcal{A}'_{1331} + \mathcal{A}'_{3311}),\\
K_{32} &= -\mathcal{A}'_{1312} - \mathcal{A}'_{3332}\,\alpha^2 - \alpha(\mathcal{A}'_{1332} + \mathcal{A}'_{3312}),\\
K_{33} &= \rho c^2 - \mathcal{A}'_{1313} - \mathcal{A}'_{3333}\,\alpha^2 - \alpha(\mathcal{A}'_{1333} + \mathcal{A}'_{3313}).
\end{aligned} \tag{A2}$$

The elasticity tensor in the initial coordinate system (x_1, x_2, x_3) exhibits the major symmetry $\mathcal{A}_{piqj} = \mathcal{A}_{qjpi}$. This symmetry persists in the rotated coordinate system (x'_1, x'_2, x'_3) after tensor transformation and as a result, K_{ij} turns out to be symmetric ($K_{ij} = K_{ji}$). Furthermore, for an initially isotropic plate subjected to a biaxial stress field in the $x_1 - x_2$ plane, the latter plane is one of mirror symmetry. This means that the strain induced anisotropy is, at least, of monoclinic symmetry. The latter symmetry is maintained in the $x'_1 - x'_2$ plane after coordinate transformation, leading to further simplification of K_{ij}

$$\begin{aligned}
K_{11} &= \rho c^2 - \mathcal{A}'_{1111} - \mathcal{A}'_{3131}\,\alpha^2,\\
K_{12} &= -\mathcal{A}'_{1112} - \mathcal{A}'_{3132}\,\alpha^2,\\
K_{13} &= -\alpha(\mathcal{A}'_{1133} + \mathcal{A}'_{3113}),\\
K_{21} &= K_{12},\\
K_{22} &= \rho c^2 - \mathcal{A}'_{1212} - \mathcal{A}'_{3232}\,\alpha^2,\\
K_{23} &= -\alpha(\mathcal{A}'_{1233} + \mathcal{A}'_{3213}),\\
K_{31} &= K_{13},\\
K_{32} &= K_{23},
\end{aligned} \tag{A3}$$

$$K_{33} = \rho c^2 - \mathcal{A}'_{1313} - \mathcal{A}'_{3333}\,\alpha^2 .$$

For non-trivial solutions to the eigenvalue problem, the determinant of K_{ij} is set to zero. This yields a sixth order equation in α which can be expressed as

$$P_6\,\alpha^6 + P_4\,\alpha^4 + P_2\,\alpha^2 + P_0 = 0 , \tag{A4}$$

where the coefficients P_6, P_4, P_2 and P_0 are given by

$$\begin{aligned}
P_6 &= \mathcal{A}'_{3333}\,\mathcal{A}'^2_{3132} - \mathcal{A}'_{3131}\,\mathcal{A}'_{3232}\,\mathcal{A}'_{3333} ,\\
P_4 &= \mathcal{A}'^2_{1233}\mathcal{A}'_{3131} + \mathcal{A}'^2_{1133}\mathcal{A}'_{3232} + \mathcal{A}'^2_{3132}\mathcal{A}'_{1313} + \mathcal{A}'^2_{3213}\mathcal{A}'_{3131}\\
&\quad + \mathcal{A}'^2_{3113}\mathcal{A}'_{3232} - 2\mathcal{A}'_{1133}\,\mathcal{A}'_{1233}\,\mathcal{A}'_{3132} + 2\mathcal{A}'_{1133}\,\mathcal{A}'_{3113}\,\mathcal{A}'_{3232}\\
&\quad - 2\mathcal{A}'_{1133}\,\mathcal{A}'_{3132}\,\mathcal{A}'_{3213} - 2\mathcal{A}'_{1233}\,\mathcal{A}'_{3113}\,\mathcal{A}'_{3132}\\
&\quad + 2\mathcal{A}'_{1112}\,\mathcal{A}'_{3132}\,\mathcal{A}'_{3333} + 2\mathcal{A}'_{1233}\,\mathcal{A}'_{3131}\,\mathcal{A}'_{3213}\\
&\quad - \mathcal{A}'_{1111}\,\mathcal{A}'_{3232}\,\mathcal{A}'_{3333} - \mathcal{A}'_{1212}\,\mathcal{A}'_{3131}\,\mathcal{A}'_{3333}\\
&\quad - \mathcal{A}'_{1313}\,\mathcal{A}'_{3131}\,\mathcal{A}'_{3232} - 2\mathcal{A}'_{3113}\,\mathcal{A}'_{3132}\,\mathcal{A}'_{3213} - \mathcal{A}'^2_{3132}\rho c^2\\
&\quad + \mathcal{A}'_{3131}\,\mathcal{A}'_{3232}\,\rho c^2 + \mathcal{A}'_{3131}\,\mathcal{A}'_{3333}\,\rho c^2 + \mathcal{A}'_{3232}\,\mathcal{A}'_{3333}\,\rho c^2,\\
P_2 &= \mathcal{A}'^2_{1233}\mathcal{A}'_{1111} + \mathcal{A}'^2_{1133}\mathcal{A}'_{1212} + \mathcal{A}'^2_{3213}\mathcal{A}'_{1111} + \mathcal{A}'^2_{3113}\mathcal{A}'_{1212}\\
&\quad + \mathcal{A}'^2_{1112}\mathcal{A}'_{3333} - 2\mathcal{A}'_{1112}\,\mathcal{A}'_{1133}\,\mathcal{A}'_{1233} - 2\mathcal{A}'_{1112}\,\mathcal{A}'_{1133}\,\mathcal{A}'_{3213}\\
&\quad - 2\mathcal{A}'_{1112}\,\mathcal{A}'_{1233}\,\mathcal{A}'_{3113} + 2\mathcal{A}'_{1133}\,\mathcal{A}'_{1212}\,\mathcal{A}'_{3113}\\
&\quad + 2\mathcal{A}'_{1111}\,\mathcal{A}'_{1233}\,\mathcal{A}'_{3213} + 2\mathcal{A}'_{1112}\,\mathcal{A}'_{1313}\,\mathcal{A}'_{3132}\\
&\quad - \mathcal{A}'_{1111}\,\mathcal{A}'_{1212}\,\mathcal{A}'_{3333} - \mathcal{A}'_{1111}\,\mathcal{A}'_{1313}\,\mathcal{A}'_{3232}\\
&\quad - \mathcal{A}'_{1212}\,\mathcal{A}'_{1313}\,\mathcal{A}'_{3131} - 2\mathcal{A}'_{1112}\,\mathcal{A}'_{3113}\,\mathcal{A}'_{3213} - \mathcal{A}'^2_{1133}\rho c^2\\
&\quad - \mathcal{A}'^2_{1233}\rho c^2 - \mathcal{A}'^2_{3113}\rho c^2 - \mathcal{A}'_{3131}\,\rho^2 c^4 - \mathcal{A}'^2_{3213}\rho c^2\\
&\quad - \mathcal{A}'_{1111}\,\mathcal{A}'_{3232}\,\rho c^2 + \mathcal{A}'_{1212}\,\mathcal{A}'_{3131}\,\rho c^2 + \mathcal{A}'_{1111}\,\mathcal{A}'_{3333}\,\rho c^2\\
&\quad + \mathcal{A}'_{1313}\,\mathcal{A}'_{3131}\,\rho c^2 - 2\mathcal{A}'_{1233}\,\mathcal{A}'_{3213}\,\rho c^2 + \mathcal{A}'_{1212}\,\mathcal{A}'_{3333}\,\rho c^2\\
&\quad + \mathcal{A}'_{1313}\,\mathcal{A}'_{3232}\,\rho c^2,\\
P_0 &= \mathcal{A}'^2_{1112}\mathcal{A}'_{1313} + \rho^3 c^6 - \mathcal{A}'_{1111}\,\mathcal{A}'_{1212}\,\mathcal{A}'_{1313} - \mathcal{A}'^2_{1112}\rho c^2 - \mathcal{A}'_{1111}\,\rho^2 c^4\\
&\quad - \mathcal{A}'_{1212}\,\rho^2 c^4 - \mathcal{A}'_{1313}\,\rho^2 c^4 + \mathcal{A}'_{1111}\,\mathcal{A}'_{1212}\,\rho c^2 + \mathcal{A}'_{1111}\,\mathcal{A}'_{1313}\,\rho c^2\\
&\quad + \mathcal{A}'_{1212}\,\mathcal{A}'_{1313}\,\rho c^2,
\end{aligned} \tag{A5}$$

The lack of odd power coefficients in equation (A4) means that the sixth order equation can be reduced to a cubic equation in α^3. This simplification results in six solutions for α, which are denoted by α_q, $q \in \{1,2,3,4,5,6\}$, with the following properties

$$\alpha_2 = -\alpha_1, \qquad \alpha_4 = -\alpha_3\,, \qquad \alpha_6 = -\alpha_5. \tag{A6}$$

For each α_q, displacement ratios $V_q = {}^{U_{2q}}\!/_{U_{1q}}$ and $W_q = {}^{U_{3q}}\!/_{U_{1q}}$ can be defined using the relations in equation (A1) as

$$V_q = \frac{K_{11}(\alpha_q)K_{23}(\alpha_q) - K_{13}(\alpha_q)K_{21}(\alpha_q)}{K_{13}(\alpha_q)K_{22}(\alpha_q) - K_{12}(\alpha_q)K_{23}(\alpha_q)},. \tag{A7}$$

$$W_q = \frac{K_{11}(\alpha_q)K_{32}(\alpha_q) - K_{31}(\alpha_q)K_{12}(\alpha_q)}{K_{12}(\alpha_q)K_{33}(\alpha_q) - K_{13}(\alpha_q)K_{32}(\alpha_q)}, \qquad q \in \{1,2,3,4,5,6\}. \tag{A8}$$

The displacement field of the Lamb waves can then be written in terms of the above displacement ratios using the principle of superposition

$$(u_1', u_2', u_3') \;= \sum_{q=1}^{6} (1, V_q, W_q)\, U_1 e^{i\xi(x_1' + \alpha_q x_3' - ct)}\;, \tag{A9}$$

Similarly, the stress field can be found by substituting the above displacement field into the incremental constitutive equation (2)

$$(\hat{S}'_{33}, \hat{S}'_{31}, \hat{S}'_{32}) = \sum_{q=1}^{6} i\xi (D_{1q}, D_{2q}, D_{3q})\, U_1 e^{i\xi(x_1' + \alpha_q x_3' - ct)}\,, \tag{A10}$$

where

$$\begin{aligned} D_{1q} &= \mathcal{A}'_{3311} + V_q \mathcal{A}'_{3312} + W_q\, \mathcal{A}'_{3333}\, \alpha_q\,, \\ D_{2q} &= \mathcal{A}'_{3131}\, \alpha_q + V_q \mathcal{A}'_{3132}\, \alpha_q + W_q\, \mathcal{A}'_{3113}\,, \\ D_{3q} &= \mathcal{A}'_{3231}\, \alpha_q + V_q \mathcal{A}'_{3232}\, \alpha_q + W_q\, \mathcal{A}'_{3213}\,. \end{aligned} \tag{A11}$$

Incorporating the relations in (A6) in equations (A7), (A8) and (A11) results in the following restrictions

$$\begin{aligned} V_{j+1} &= V_j\,, \\ W_{j+1} &= -W_j\,, \\ D_{1j+1} &= D_{1j}\,, \\ D_{2j+1} &= -D_{2j}, \\ D_{3j+1} &= -D_{3j}, \qquad j = 1,3,5\,. \end{aligned} \tag{A12}$$

In order to satisfy the incremental traction-free boundary conditions at the upper and lower surfaces of the plate, the components of the incremental nominal stress must be set to zero

$$\hat{S}'_{31} = \hat{S}'_{32} = \hat{S}'_{33} = 0 \text{ at } x'_3 = \pm h/2\,. \tag{A13}$$

This leads to a system of equations which can be expressed as

$$i\xi \begin{pmatrix} D_{11}E_1 & D_{12}E_2 & D_{13}E_3 & D_{14}E_4 & D_{15}E_5 & D_{16}E_6 \\ D_{21}E_1 & D_{22}E_2 & D_{23}E_3 & D_{24}E_4 & D_{25}E_5 & D_{26}E_6 \\ D_{31}E_1 & D_{32}E_2 & D_{33}E_3 & D_{34}E_4 & D_{35}E_5 & D_{36}E_6 \\ D_{11}\overline{E_1} & D_{12}\overline{E_2} & D_{13}\overline{E_3} & D_{14}\overline{E_4} & D_{15}\overline{E_5} & D_{16}\overline{E_6} \\ D_{21}\overline{E_1} & D_{22}\overline{E_2} & D_{23}\overline{E_3} & D_{24}\overline{E_4} & D_{25}\overline{E_5} & D_{26}\overline{E_6} \\ D_{31}\overline{E_1} & D_{32}\overline{E_2} & D_{33}\overline{E_3} & D_{34}\overline{E_4} & D_{35}\overline{E_5} & D_{36}\overline{E_6} \end{pmatrix} \begin{pmatrix} U_{11} \\ U_{12} \\ U_{13} \\ U_{14} \\ U_{15} \\ U_{16} \end{pmatrix} e^{i\xi(x'_1 - ct)} = \begin{Bmatrix} 0 \\ 0 \\ 0 \\ 0 \\ 0 \\ 0 \end{Bmatrix}, \tag{A14}$$

where $U_{1q} = U_1(\alpha_q), E_q = e^{i\xi\alpha_q\frac{h}{2}}$ and $\overline{E_q} = e^{-i\xi\alpha_q\frac{h}{2}}$.

For non-trivial solutions, the determinant of the coefficient matrix in (A14) must go to zero. Using row and column operations along with the symmetries in (A12), the determinant can be reduced to two characteristic equations

$$\begin{aligned} D_{11}G_1\cot(\zeta\alpha_1) - D_{13}G_3\cot(\zeta\alpha_3) + D_{15}G_5\cot(\zeta\alpha_5) &= 0 \\ D_{11}G_1\tan(\zeta\alpha_1) - D_{13}G_3\tan(\zeta\alpha_3) + D_{15}G_5\tan(\zeta\alpha_5) &= 0\,, \end{aligned} \tag{A15}$$

corresponding to symmetric and anti-symmetric modes respectively, with

$$\begin{aligned} G_1 &= D_{23}D_{35} - D_{25}D_{33}\,, \qquad G_3 = D_{21}D_{35} - D_{25}D_{31}\,, \\ G_5 &= D_{21}D_{33} - D_{23}D_{31}\,, \qquad \zeta = \frac{\xi h}{2} = \frac{\omega h}{2c}\,. \end{aligned} \tag{A16}$$

Appendix B

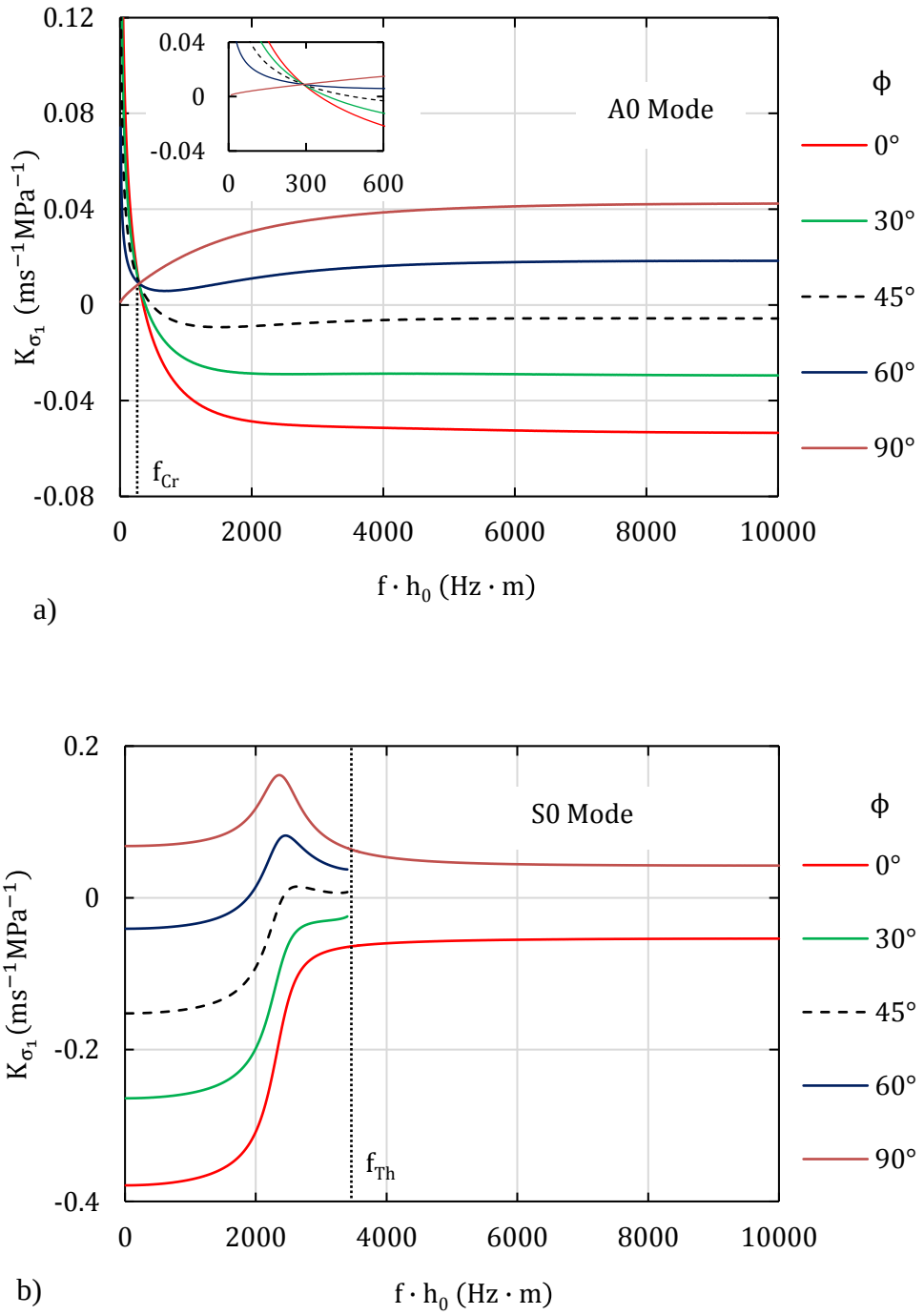

Figure A1. Variation of the coefficient relating changes in C_p to the applied stress σ_1 for the (a) A0 mode and, (b) S0 mode, at different angles of wave propagation, ϕ (measured relative to the σ_1 direction).